This is a peer-reviewed, accepted author manuscript of the following research article: Hu, L, Zhang, M, Li, G, Yuan, Z, Bi, J & Guo, Y 2024, 'Multi-objective model predictive control for ship roll motion with gyrostabilizers', Ocean Engineering, vol. 313, no. Part 1, 119412. https://doi.org/10.1016/j.oceaneng.2024.119412

Multi-objective model predictive control for ship roll motion with gyrostabilizers

Lifen Hu[1], Ming Zhang[2], Gang Li[3], Zhiming Yuan[4], Junying Bi[1], Yanli Guo[1]

1. Ulsan Ship and Ocean College, Ludong University, Yantai 264025, China; 2. National Key Laboratory of Autonomous Marine Vehicle Technology, Harbin Engineering University, Harbin 150001, China; 3. Transportation School, Ludong University, Yantai 264025, China; 4. Department of Naval Architecture, Ocean and Marine Engineering, University of Strathclyde, Glasgow G4 0LZ, UK

Abstract:

Ships are prone to significant roll motion while sailing in adverse conditions, posing a serious threat to ship safety and maneuverability. Therefore, effective ship motion control is crucial. Integrating the MPC control algorithm with a gyrostabilizer can effectively achieve this goal. To evaluate and compare control strategies, a multi-objective model predictive control is proposed that integrates considerations of ship motion, safety, and energy consumption to conduct the operation concurrently. By assigning different weights to these factors, the study aims to discern the varying impacts on control effectiveness. The response of ship roll motion in beam waves is evaluated through roll hydrodynamic modelling, accounting for wave memory effects. A state-space model of ship and gyrostabilizers is proposed to represent their dynamic interaction and response to external moment. Subsequently, the influence of different weightings in the multi-objective model predictive control is compared, and the control performances of a frigate under different wave conditions are analyzed respectively. The multi-objective model predictive control, with varied weight assignments, leads to distinct reductions in roll motions. This investigation offers valuable insights into controlling roll motion in beam wave conditions, effectively reducing motion under varying sea conditions, and providing alternative guidance tailored to user preferences.

Keywords: roll motion control; irregular wave; model predictive control; gyrostabilizer

1 Introduction

The motion of ships can be significantly affected by rolling during tough weather conditions, which can seriously impact safety and pose considerable risks to maneuvering operations. Therefore, effectively controlling the motion of the ship is crucial. The previous research has predominantly concentrated on performance optimization of hydrodynamic equipment and ship safety improvement in the design phase [Irkal, 2019; Kang, 2013], addressing realistic sea conditions with random wave frequencies and directions presents challenges. In these scenarios, eliminating roll motion may not be realistically achievable. However, the adoption of a reasonable strategy or system for controlling ship motions in waves could greatly enhance ship safety.

Recently, there has been a lot of research on different real-time control techniques for ship motion [Li, 2016a; Liu, 2020]. When it comes to controlling the roll motion of a ship, it's crucial to have data about the excitation moment. There are two main methods for obtaining information about the wave excitation moment: one is using CFD (Computational Fluid Dynamics), which calculates the NS (Navier–Stokes) equations taking into account fluid viscosity and the nonlinear interaction of the ship and the wave [Gao, 2020; Hu, 2021]. However, the method requires excessive computational time to achieve more accurate results. The alternative method, known as potential flow theory, it relies on the Laplace equation and does not take into account viscous effects [Li, 2016b; Li, 2019]. It determines the total wave moment by integrating pressure across the wet surface

over time. Additionally, based on the same foundational theory, the impulse response theory was proposed to precisely analyze ship motion response [Cummins, 1962]. This theory represents wave radiation moment as a convolution term, albeit at the cost of reduced calculation efficiency. Subsequently, the state space function was introduced as a replacement for the impulse response model and has been widely used to enhance calculation efficiency [Taghipour, 2008; Zhang, 2024], thus demonstrating a significant improvement in analysis efficiency [Zhang, 2016].

On the other hand, the roll stabilization devices as external systems insignificantly affect the lightweight of ship. However, they are susceptible to damage and might lose effectiveness when the vessel is not in motion [Townsend, 2014]. In contrast, internal systems represented by the gyrostabilizer, do not contribute to the increased hydrodynamic resistance and are notably effective even when the vessel is stationary. The gyrostabilizer remains effective irrespective of its position within the hull. Although it has demonstrated excellent performance in certain sailing conditions, reducing roll by up to 95% (RMS) at most [Palraj, 2020], its application has been restricted due to the high cost and the absence of adequate controls to sustain performance. Recent innovations in materials, mechanical engineering, and control systems have enabled effective utilization of gyrostabilizers for enhanced roll motion control and stability in marine vehicles such as yachts [Takeuchi, 2011]. These advancements in control systems facilitate real-time monitoring and adjustment of dynamic characteristics [Perez, 2009a]. Moreover, experimental studies on barges demonstrate that gyrostabilizers can reduce roll motion by nearly half [Palraj, 2021]. However, the results suggest that the gyrostabilizer has already reached its limitations based on existing control algorithms. To fully develop its potential in control performance, integrating the gyrostabilizer with robust control algorithms presents a promising approach to maximizing its control performance potential and finding practical solutions for non-linear systems [Tiwari, 2021].

Control algorithms play a crucial role in optimizing ship motion. In response to challenges posed by nonlinear dynamics induced by waves, researchers have extensively explored the traditional PID control method for its straightforward structure and ease of tuning [Tomera, 2017; Hu, 2023a]. However, it struggles with the complexities of nonlinear dynamics caused by turbulent waves. Fortunately, advancements have led to the development of intelligent algorithms, among which LQR (linear quadratic regulator) and MPC (model predictive control) stand out as optimal methods [Pascoal, 2005]. Despite their effectiveness, PID and LQR may falter in scenarios involving time delays and can exacerbate oscillations when encountering input or rate saturation issues [Lee, 2011]. The PID control algorithm combined with an active gyrostabilizer is proposed to adjust roll motion using precession angle input [Song, 2023], comparative results show that the active gyrostabilizer can markedly decrease the amplitude of rolling resonance compared to the passive gyrostabilizer. On the other hand, MPC is particularly promising because it integrates disturbance rejection, manages constraints, handles slow-moving dynamics, and incorporates energy conservation strategies into its controller design, making it better suited for nonlinear systems and system delays [Li, 2018]. MPC has seen increasing applications in sophisticated engineering control [Kang, 2021], including path following [Sandeepkumar, 2022], the vibration of platform [Ma, 2022], autonomous ship avoidance [Zhang, 2022], dynamic positioning [Li, 2017], roll motion stabilization [Jimoh, 2021], and room temperature control [Aswani, 2012]. These results demonstrate effectiveness and achieve fast dynamic responses with strong robustness. Among these, the cost function directly affects control performance. For instance, in the room temperature control application using MPC, a dual-objective cost function was employed. The first objective minimized the squared tracking error between the room temperature and the setpoint across the control horizon. The second objective focused on optimizing energy consumption throughout the control period based on the control inputs. Similarly, a disturbance rejection

MPC strategy is implemented to dampen vertical motions of a passenger ship [Kucukdemiral, 2019], where the cost function focused on minimizing tracking error and control signal change with evenly assigned weightings. While these cost functions efficiently addressed single or two-term objectives to achieve optimal solutions, they often overlooked the inherent complexity in balancing multiple competing objectives simultaneously. This limited their flexibility in evaluating alternatives under varying conditions.

When applied to ship motion control environments, integrating MPC with gyrostabilizer for motion control is highly feasible and beneficial, which has been applied successfully in a single-track vehicle [Chu, 2017]. MPC, known for its ability to handle complex dynamics and optimize control inputs, can utilize angular velocity data from gyrostabilizer as key state variables or observation inputs. This incorporation allows MPC to make more accurate predictions about future system states. Additionally, the real-time feedback provided by gyrostabilizer enables MPC to continuously update and refine its model, which enhances prediction accuracy and system responsiveness. The combination of these technologies results in improved control precision, better handling of dynamic changes, and overall enhanced performance in motion control applications. For roll motion control analysis, previous studies focused solely on the roll angle as the cost function [Hu, 2023b]. With the circumstance that the roll angle is less than 5 degrees, the system activates, potentially impacting energy efficiency. So on the basis of combining MPC method with gyrostabilizer, this paper proposes a unique cost function aimed at adjusting the ship roll motion according to user requirement. This adjustment transforms roll motion control into a multi-objective model predictive control problem, allowing for a more comprehensive balance of different motion control objectives. This approach is suggested to offer more practical and balanced roll control solutions [Shu, 2024]. Notably, the study simultaneously considers three key factors: ship motion, safety, and energy consumption, a relatively rare approach in prior research. The cost function in this study is constructed by integrating several motion-related objectives:

(1) To maintain the roll angle within a safe limit: This objective prioritizes keeping the ship's roll within a predefined safe range to ensure stability and prevent excessive rolling, which can pose risks to the vessel.
(2) To avoid damage to the hull structure: This objective aims to protect the integrity of the ship's hull to avoid potentially structural damage or fatigue, ensuring the vessel's long-term structural health and safe.
(3) To minimize the energy loss as much as possible: Energy efficiency is crucial in reducing operational costs. Minimizing control moment can help reduce energy losses associated with excessive gyrostabilizer motions, contributing to overall fuel savings and environmental sustainability.

By incorporating these objectives into the cost function, the study seeks to achieve a balanced approach to ship roll motion control, considering both safety and efficiency concerns. According to the principles of optimal control, MPC method is employed to derive control strategies and implement them in real-time adjustments of the gyrostabilizer, aligning its motion with the ship’s movement. This study primarily focuses on optimizing roll motion while prioritizing ship safety and minimizing energy consumption. Here are the highlighted contributions of this work:

(1) Introduction of a unique cost function: The proposed cost function integrates considerations of ship motion, safety, and energy consumption. By incorporating these diverse factors, it provides a more comprehensive evaluation of control effectiveness. This approach enables smoother adjustments based on the controller's decisions, enhancing overall control performance.

(2) Weighting analysis of factors: Different weights are assigned to the aforementioned factors to compare their respective influences on control ability. Through this analysis, the most sensitive factor in motion control will be identified, facilitating targeted improvements in control strategies.

(3) Proposing a multi-objective model predictive control: Integrating the multi-objective model predictive control with gyrostabilizer and wave memory effect collectively enables the robust handling of nonlinear dynamic models, developing a precise and highly effective control strategy.

This study presents a theoretical framework for employing multi-objective model predictive control to stabilize the roll motion of ships. The following sections are organized as follows: Section 2 details the ship roll control framework. Section 3 introduces a method using multi-objective model predictive control. Section 4 includes a case study analyzing different beam wave conditions, accompanied by plausible explanations. Conclusions are summarized in Section 5.

2 Gyrostabilizer and roll motion control combination

The gyrostabilizer operates on the principle of the conserving angular momentum, effectively controlling a ship's motion, its key component are depicted in Fig. 1. In a single-axis gyrostabilizer, the flywheel is spun around its axis by a motor. This rotation allows it to resist changes in orientation caused by external moment. Once connected to the ship, the gyrostabilizer counters rolling by limiting the flywheel's rotation. When a steady external moment or angular speed acts, its axis precesses, maintaining constant angular motion perpendicular to the external moment. Despite being installed in the hull, the gyrostabilizer offers efficient use of space utilization compared to other devices and is easy to maintain.

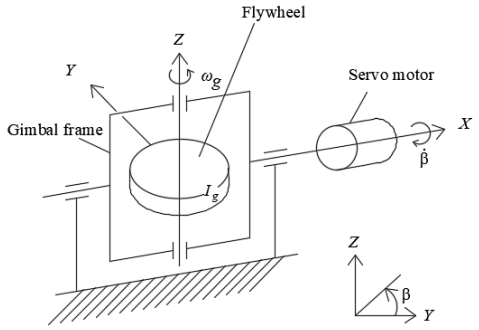

Fig. 1 Sketch of gyrostabilizer system of active control.

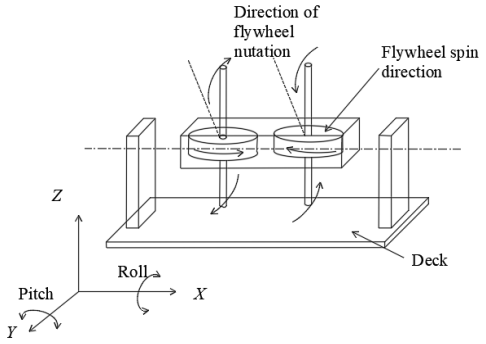

Fig. 2 Arrangement of dual gyrostabilizers.

The gyrostabilizer include passive and active depending on how the flywheel spin axis is oriented. Active gyrostabilizers, as utilized in this study, demonstrate superior performance by actively controlling the precession torque regardless of operating conditions, thereby enhancing gyro efficiency [Palraj, 2020]. Fig. 1 illustrates the schematic of an active gyrostabilizer. However, relying solely on a single gyrostabilizer to generate control moments can pose issues. Variations in flywheel nutation direction and output moment may cause unexpected ship movements such as unnecessary yaw or pitch. To mitigate this, dual-flywheel setups spin in opposite directions to prevent ship motion around the precession axis [Townsend, 2007], just depicted in Fig. 2. Both flywheels spin at equal speeds but opposite directions, cancelling out undesired torques like pitch and yaw while doubling the control roll moment. The gyrostabilizer is designed to fit within the ship's inner hull dimensions and is positioned along the centerline to align closely with the ship's center of gravity, with the gimbal axis consistently perpendicular to the direction of the waves.

According to the impulse response theory [Cummins, 1962], roll motion typically emerges as the predominant factor in beam seas, a phenomenon extensively explored in prior research [Hinostroza, 2015; Jimoh, 2021]. Thus, the well-known roll motion model and the precession motion with gyrostabilizers can be explained in the following:

$$\begin{aligned} I_s\ddot{\phi}(t)+\int_0^t h(t-\tau)\dot{\phi}(\tau)d\tau+K\phi(t)&=M_{wave}(t)\text{-}M_{gs}(t)\\ I_g\ddot{\beta}(t)+B_g\dot{\beta}(t)+C_g\beta(t)&=I\omega_g\dot{\phi}(t)\cos\beta(t)+M_c(t)\end{aligned}, \tag{1}$$

where I_s denotes the mass moment of inertia of the ship; $\phi(t)$, $\dot{\phi}(t)$, $\ddot{\phi}(t)$ represent the vessel's roll angle, velocity, and acceleration, respectively; K signifies the coefficient for restoring the ship's roll moment. Given the complexity of the nonlinear restoring moment solution, a piece wise method is used to linearize it to reduce calculation time [Hu, 2018]. Consequently, K is approximated as a linear function of $\phi(t)$; and h stands for the fundamental function for delay in the time-domain, reflecting the memory effect of the free surface, it can be obtained either from the added mass $J_{xx}(\omega)$ or the potential damping $B(\omega)$ in the frequency domain [Hu, 2023b]; $M_{gs}(t)=-mI\omega_g\dot{\beta}(t)\cos\beta(t)$ is the reactive moment of gyrostabilizer; here, $m=2$; $M_c(t)$ denotes the control moment; I_g represents the inertia of the spinning flywheel around the precession axis; I denotes the polar moment of inertia relative to the reference point; ω_g represents the spin angular velocity; B_g is the frictional damping coefficient; C_g stands for the restoring coefficient influenced by the spinning flywheel's mass distribution; $\beta(t)$, $\dot{\beta}(t)$, $\ddot{\beta}(t)$ is the angle of precession, its velocity and acceleration respectively. The control moment $M_c(t)$ is considered as the manipulated variable, and $\phi(t), \dot{\phi}(t), \beta(t), \dot{\beta}(t)$ are referred to as states. $M_{wave}(t)$ represents the wave excitation moment that is calculated by potential theory and expressed as follows:

$$M_{wave}(t)=M_{F-K}(t)+M_d(t), \tag{2}$$

where $M_{F-K}(t)$ represents the Froud–Krylov (F-K) moment; $M_d(t)$ signifies the diffraction moment generated by the wave passing through the floating body [Suner, 2022; Bu, 2020]. In the scenario of beam waves, $M_{wave}(t)$ is calculated based on the Froud–Krylov hypothesis. The sea condition adopted in the paper is the JONSWAP wave spectrum, widely acknowledged as representative of conditions where the majority of marine vessels operate.

3 Model predictive control

3.1 MPC theory

The left plot of Fig. 3 outlines the MPC control diagram. At each discrete sampling instant, the optimization computes increments that minimize the cost function within current constraints. This optimization predicts the controlled variable based on the current state vector. It then executes the optimal input, reassesses the system's state, and updates the plant's current state with the optimal control input [Fossen, 2011]. MPC systems consist of key components: a system model, a cost function, constraints, an optimization method, and a control horizon, all of which impact the control performance. MPC calculates the applied input using predicted system behavior,

accommodating state constraints and optimizing the specified cost function [Findeisen, 2002]. In MPC, the system model is used to generate a control vector by minimizing a specified cost function while considering disturbances and constraints [Afram, 2014; Ławryńczuk, 2023]. The cost function can encompass factors like control effort, energy cost, or power consumption [Ławryńczuk, 2023]. Constraints are applied to actuators' limits and variables. The controller simulates predicted system responses to compute the control vector, effectively regulating processes within defined limits. Therefore, nonlinear MPC enables precise decision-making, rendering it a widely used predictive control strategy in real-time scenarios.

The right plot of Fig. 3 is the detailed flowchart of MPC working principle. Firstly, the initialization gives the state, objective, constraints, initial condition and et al. Then it defines the system model, formulates the optimization problem, solves the problem to get control inputs, and finally applies these inputs to the system while updating state and model. This study employs the nonlinear MPC method for ship motion controlling in different waves. Sections 3.2 and 3.3 provide detailed discussions on the state space representation and cost function, respectively.

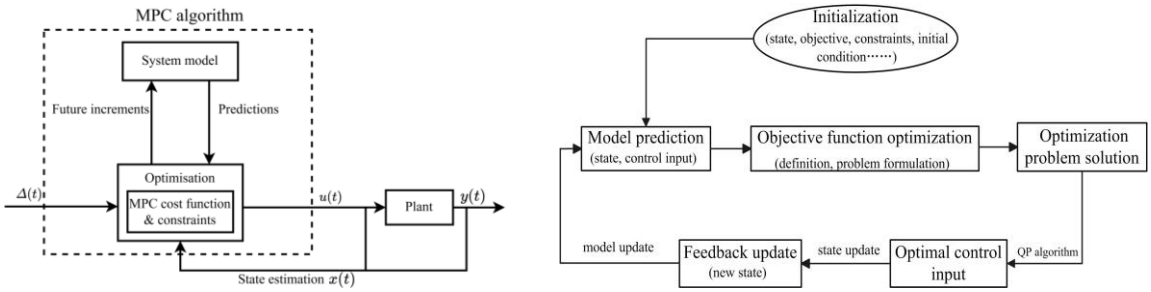

Fig. 3 Detailed description of MPC method (left) closed loop control; (right) flowchart of MPC control

3.2 State space representative

Eq.(1) presents challenges for control strategy implementation due to the integral form of the radiation moment, so it utilizes frequency domain identification methods for improved accuracy [Zhang, 2024; Perez, 2009b]. This dynamic model integrates states, memory effects, and manipulated variables into a state-space representation, as demonstrated in Eq. (3).

$$\begin{aligned} &I_s\ddot{\phi}(t)+\boldsymbol{C}\boldsymbol{u}(t)+K\phi(t)=M_{wave}(t)\text{-}M_{gs}(t)\\ &I_g\ddot{\beta}(t)+B_g\dot{\beta}(t)+C_g\beta(t)=I\omega_g\dot{\phi}(t)\cos\beta(t)+M_c(t),\\ &\dot{\boldsymbol{u}}(t)=\boldsymbol{A}\cdot\boldsymbol{u}(t)+\boldsymbol{B}\cdot\dot{\phi}(t) \end{aligned} \tag{3}$$

where $\boldsymbol{u}(t)\in R^{n\times 1}$ is the state vector incorporating the memory effect caused by the free surface; $\boldsymbol{A}$, $\boldsymbol{B}$, $\boldsymbol{C}$ are the state-space representation derived directly from the transfer function. These representations are estimated using system identification method [Taghipour, 2008; Hu, 2023b], which is not addressed in this paper.

A state vector is defined as $\mathbf{x}(t)=[\phi(t),\dot{\phi}(t),\beta(t),\dot{\beta}(t),\mathbf{u}(t)^T]^T\in R^{(n+4)\times 1}$. Then, Eq. (3) can be rewritten as

$$\dot{\mathbf{x}}(t)=\gamma\cdot\mathbf{x}(t)+\eta(t)$$
$$\gamma=\begin{bmatrix} 0 & 1 & 0 & 0 & \mathbf{0} \\ -\frac{K}{I_s} & 0 & 0 & -\frac{M_{gs}(t)}{I_s} & \mathbf{B} \\ 0 & 0 & 0 & 1 & \mathbf{0} \\ 0 & \frac{I\omega_g}{I_g} & -\frac{C_g}{I_g} & -\frac{B_g}{I_g} & \mathbf{0} \\ \mathbf{0} & \mathbf{C} & \mathbf{0} & \mathbf{0} & \mathbf{A} \end{bmatrix},\ \eta(t)=\begin{bmatrix} 0 \\ \frac{M_{wave}(t)}{I_s} \\ 0 \\ \frac{M_c}{I_g} \\ \mathbf{0} \end{bmatrix}. \tag{4}$$

Eq. (4) serves as an analytical Jacobian matrix within the prediction model, significantly enhancing simulation efficiency and streamlining the implementation of the control algorithm. Initial conditions are necessary for solving Eq. (4), utilizing a fourth-order Runge-Kutta method with a system order of n=4. This study focuses on motion control simulation, encompassing eight states and one manipulated variable.

3.3 Cost functions and constraints

In MPC, the cost function and constraints, as depicted in Fig. 3, are fundamental. The approach involves tackling the problem over a finite horizon, ensuring real-time adaptability in a receding horizon manner. The cost function is fundamental as it defines the desired system behaviour, crucial for stabilizing the system and achieving specific performance targets. In ship motion control systems, objectives such as minimizing energy consumption, preventing ship structure damage, and reducing roll motion often compete with each other. A trade-off is achieved by assigning weights to these factors within the cost function. In the quadratic cost function typically used in MPC, these weights determine the balance between control effort and control error. This ensures that the control action is both effective and efficient, aligning with operational goals. To assess the impact of control strategies, a multi-objective cost function as detailed in Eq. (5) and Eq. (6) are employed. This function provides a comprehensive evaluation of control performance, considering various influences pertinent to MPC methodologies.

$$\begin{aligned} &\min J_c(\mathbf{x}_{\_n}(t),\eta_{\_n}(t);T_p,T_s) \\ &\quad J_c=F(\mathbf{x}_{\_n}(t),\eta_{\_n}(t);T_p,T_s) \\ &\quad =\sum_{t=1}^{N}(k_1\cdot\left\|\mathbf{x}_{\_n1}(t)-\mathbf{x}_{\_n1}(s)\right\|_Q^2+k_2\cdot\left\|\mathbf{x}_{\_n4}(t)-\mathbf{x}_{\_n4}(s)\right\|_R^2+k_3\cdot\left\|\eta_{\_n1}(t)-\eta_{\_n1}(s)\right\|_M^2) \end{aligned}, \tag{5}$$

where $\|*\|^2=(*)^T(*)$ denotes the Euclidean vector norm, T_p is the prediction horizon of MPC and T_s is the sample time; the semicolon ";" within a function argument indicates that the following symbols should be interpreted as additional parameters, i.e. $f(\mathbf{z};\gamma)$ means the value of the function f at $\mathbf{z}$ with the parameter γ. $\mathbf{x}_{\_n1}(t)$, $\mathbf{x}_{\_n4}(t)$ represent the roll angle and reactive moment excited on the ship after orthogonalization, respectively. $\eta_{\_n1}(t)$ denotes the control moment excited on the gyrostabilizer after orthogonalization. $\mathbf{x}_{\_n1}(s)$, $\mathbf{x}_{\_n4}(s)$ and $\eta_{\_n1}(s)$ correspond to given setpoints, which are the desired state vector parameters. The matrices *Q*, *R*, and *M* are selected as positive semi-definite matrices, as indicated in Table 1.

The first term in J_c represents the squared sum of the control error, indicating the difference between

actual roll and desired roll over the control horizon. The second term is intended to mitigate potential ship structure damage, represented by reactive moment. The third term signifies the control moment applied to the gyrostabilizer, which directly impacts energy consumption in active control systems. Efforts to optimize energy consumption in gyrostabilizers often focus on balancing the effectiveness of the control moment in reducing roll motion with the overall energy efficiency of the system. This balance ensures improved ship stability without unnecessary energy consumption, enhancing vessel performance and sustainability. Additionally, minimizing large control moments is crucial as they may pose risks to the ship's structure. Each term of the function J_c employs square norms due to the beneficial numerical properties they confer to the entire MPC optimization task. J_c represents the comprehensive cost function that integrates these three factors, each assigned different weights k_1, k_2 and k_3, subject to specific constraints outlined in Eq. (6). A higher value of k_1 signifies greater emphasis on controlling roll motion and achieving minimal roll angles, potentially increasing the control moment and leading to ship structure damage.

$$\begin{aligned} s.t. \quad & \dot{\mathbf{x}}_{\_n}(t) = \gamma \cdot \mathbf{x}_{\_n}(t) + \eta_{\_n}(t) \\ & N = T_p / T_s \\ & \mathbf{x}_{\_n}(t) \in [x_l, x_u] \\ & \sum_{i=1}^{3} k_i = 1, \; k_i \in [0,1] \\ & \mathbf{x}_{\_n}(0) = \mathbf{x}_{initial} \end{aligned} \quad , \tag{6}$$

where the initial constraint involves the permissible states of the ship and the gyrostabilizer's hydrodynamic characteristics within the system's space. The subsequent constraint deals with the relation among calculation timestep, prediction horizon and the sample time. The third constraint concerns boundary conditions for the states, where the subscripts *l* and *u* denote lower and upper bounds, respectively. The fourth constraint establishes relationships between different weights and their permissible ranges. The final constraint ensures that the initial state of the roll motion control equation meets the required condition.

Considering that accuracy and stability are sufficient in the simulation, the sample time T_s is set to 0.1 s. Additionally, to ensure desired control performance, both the prediction time and control time should be kept relatively short, the prediction horizon T_p is 50 s. The matrices *Q*, *R*, and *M* choice depends on the magnitude relationships between the elements considered in the cost function. The limitation of states and weights interval are obtained by interviewing with the experts in the gyrostabilizer and control domain. Also The MPC controller is implemented using the MATLAB Model Predictive Controller Toolbox, offering users flexibility to customize parameters such as the cost function and state space. The dynamic optimizer module is utilized by default. All computations are performed on a 16-core (Intel Xeon, 2.4 GHz) server computer.

Table 1 MPC controller parameters

Particulars	**Value**
T_s	0.1 s
T_p	50 s
Q	diag([1 0 0 0 0 0 0 0])
R	diag([0 0 0 0.01 0 0 0 0])
M	diag([0 0 0 0.01 0 0 0 0])

4 Case study

The frigate DTMB 5415 is adopted as the test ship for analysis. The calculated coefficients, including added mass $J_{xx}(\omega)$, potential damping $B(\omega)$ and others are acquired through system identification [Hu, 2023b]. Table 2 provides the primary data concerning the DTMB 5415 and the gyrostabilizer, respectively.

Table 2 Main data of DTMB 5415 and gyrostabilizer

Objective	**Particulars**	**Value**
DTMB 5415	Length of all (L_{oa}) (m)	153.300
	Length of perpendicular (L_{pp}) (m)	142.200
	Breath of waterline (B_{wl}) (m)	19.074
	Depth (D) (m)	12.470
	Draft (T) (m)	6.150
	Displacement (Δ) (m^3)	8424
	Metacentric height (GM) (m)	1.938
	Centre of gravity above base line (KG) (m)	7.555
	Roll radius of gyration (k_{xx}-water) (m)	6.932
	Pitch and yaw radius of gyration (k_{yy}-air) (m)	36.802
gyrostabilizer	Transverse inertia moment I_g ($t \cdot m^2$)	20000
	Polar inertia moment I ($t \cdot m^2$)	40000
	Damping B_g ($t \cdot m^2/s$)	50422.81
	Restoring moment C_g ($t \cdot m^2/s^2$)	435.03
	Speed of revolution ω_g (rpm)	400
	Mass (t)	53

4.1 Validation of state-space model

The performance of MPC control is validated by comparing with existing literature. The initial hydrodynamic coefficients are cross-checked against those estimated using the state matrices, affirming the reliability of the parameters utilized in the state-space model. Moreover, the roll RAO with different wave frequencies calculated by AQWA with experimental data are shown in Fig. 4 [Begovic, 2013], where ϕ represents the roll amplitude, k and A are the wave number and wave amplitude, ω and L_{PP} are the wave frequency and the ship length, respectively; g denotes the acceleration due to gravity. The comparison between numerical simulation and experiment suggests qualitative confirmation of the computational findings. Furthermore, when the dynamic system of the MPC model receives no control command, the roll motion control model's response is solely driven by the wave moment. The results indicate a slight discrepancy between the response simulations of the hydrodynamics model and the state-space model, with a maximum error of 5%, as depicted in Fig. 5.

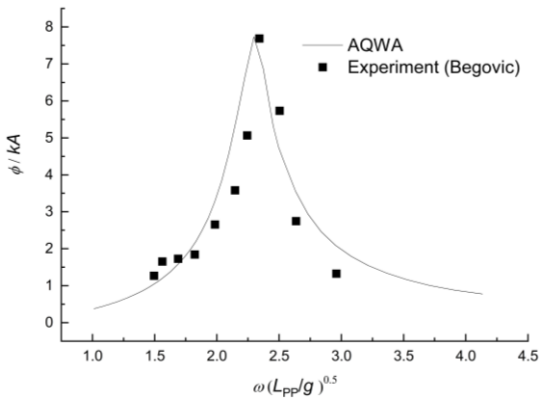

Fig. 4 Comparison of roll RAO.

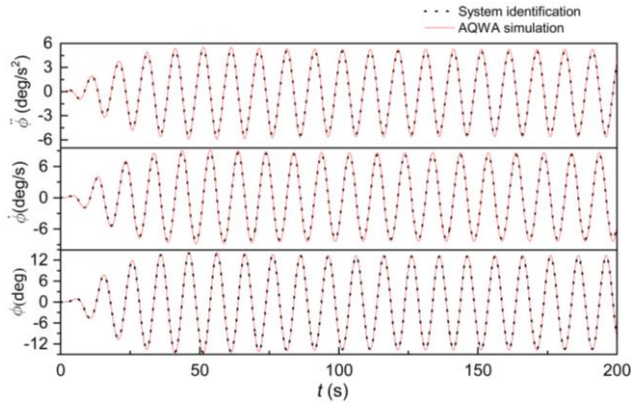

Fig. 5 Roll motion response result (regular wave, ω=1.227 rad/s; H =0.817).

On the other hand, the proposed MPC with gyrostabilizer control for a specific ship under irregular sea waves is validated against existing literature [Liu, 2022]. The wave condition follows a JONSWAP spectrum with a significant wave height of 2m, depicted in Fig. 6, and the roll motion control is achieved using an active gyrostabilizer. Fig. 7 illustrates the active control activities for different considered methods. Table 3 highlights that the maximum roll magnitude decreases from 14.523 degrees to 1.610 degrees and 0.303 degrees, respectively. Similarly, the roll angle standard deviation reduces from 7.244 degrees to 0.780 degrees and 0.073 degrees, indicating reductions of approximately 89.22% and 98.74%, with the gyrostabilizer alone and the combination of gyrostabilizer and MPC method, respectively. That is, with the application of the gyrostabilizer [Liu, 2022], only 10% standard deviation remains, whereas the current method achieves a standard deviation of just 1%.

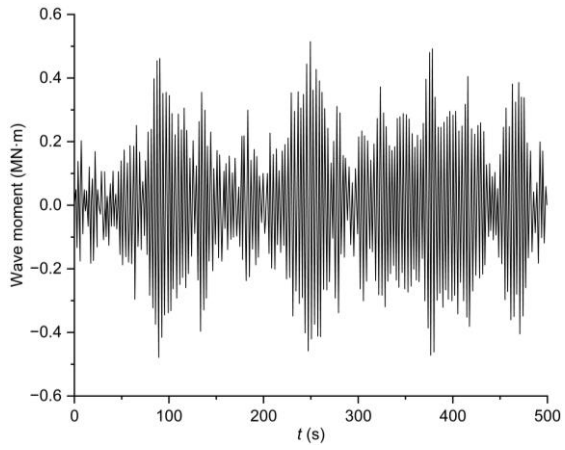

Fig. 6 Irregular wave moment (irregular wave, H_S =2m).

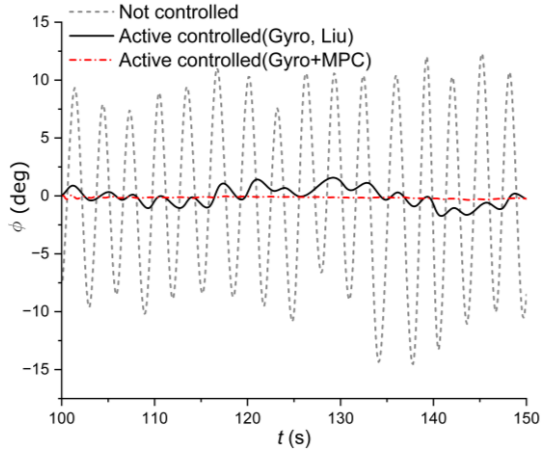

Fig. 7 Roll motion result comparison for different stages.

Table 3 Roll amplitude comparison

Particulars	**Without control**	**Gyrostabilizer [Liu, 2022]**	**MPC+gyrostabilizer (Present method)**
Maximum roll magnitude (deg)	14.523	1.610	0.303
Mean roll magnitude (deg)	-0.196	-0.050	-0.148
Roll angle standard deviation (deg)	7.244	0.780	0.073

4.2 Case study with regular wave

Table 4 Wave parameters

Wave type	Wave parameters	Value
Regular beam wave	ω (rad/s)	0.614
	H (m)	3.269
	T (s)	10.228

A study is conducted to compare the effects of different weights on ship roll motion control. The wave parameters are detailed in Table 4. The study considers cases for both regular and irregular beam waves, as shown in Fig. 8, where the green background are the calculated cases, and the black line is the boundary of the scenarios. In total, there are 36 scenarios corresponding o different combination of assigned weights k_1, k_2 and k_3. When the initial condition is k_1=0 and k_2=0, the system operates under original hydrodynamics calculations without control. Conversely, setting k_1=1 replicates the previous investigation where only roll angle is considered in the cost function. Therefore, varying k_1 from 0 to 1 spans between these two conditions.

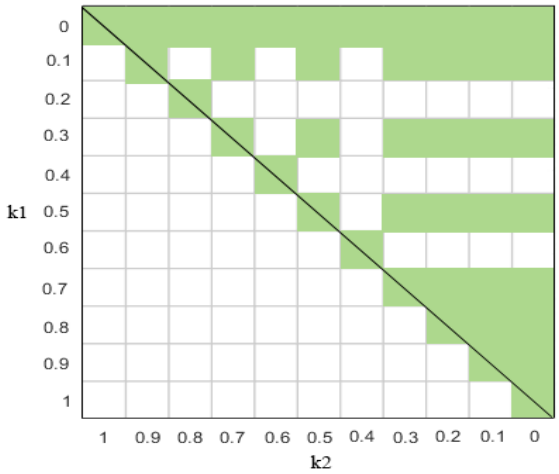

Fig. 8 Case study under regular and irregular wave.

Fig. 9 illustrates the roll angle changes with k_2 when $k_1=0.1$. On the left, the roll angle varies between approximately -4.0 degrees to 4.0 degrees, decreasing as k_2 increases. At $k_2=0.9$, the average peak value reaches a minimum of about 0.329 degrees. The results of maximum magnitudes and peak averages of roll angle are presented in Table 5. Due to the regular wave condition, the time-domain average of the roll angle is small, thus the peak average is utilized for comparative control results. A similar trend is observed for $k_1=0.7$ in Fig. 10, where the roll angle ranges from -2.5 degrees to 2.5 degrees, with the smallest amplitude occurring at $k_2=0.3$. For any k_1 value ranging from 0.1 to 1.0, the trend indicates that the roll angle decreases to a minimum as k_2 increases, under the condition $k_1+k_2\leq 1$. The reason could be attributed to the weight assignment in Eq. (6), with a fixed weight of k_1 on the roll angle, an increasing k_2 implies a greater reactive moment and reduced weight of the control moment. For $k_1=0.1$ in Table 5, the roll angle decrease with increasing k_2, until $k_2=0.9$, where the weight of k_3 is 0, indicating no constraint on the control moment.

Consequently, the control moment, represented by the precession angle, maximizes to achieve the minimal roll angle. This trend persists regardless of the k_1 value chosen.

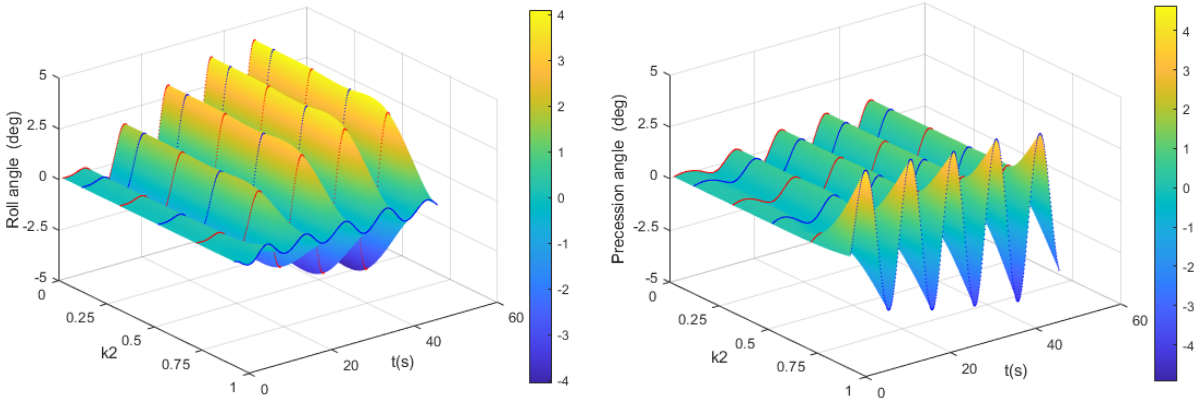

Fig. 9 Roll angle and precession angle amplitude change with k_2 for k_1=0.1 (left) roll angle; (right) precession angle.

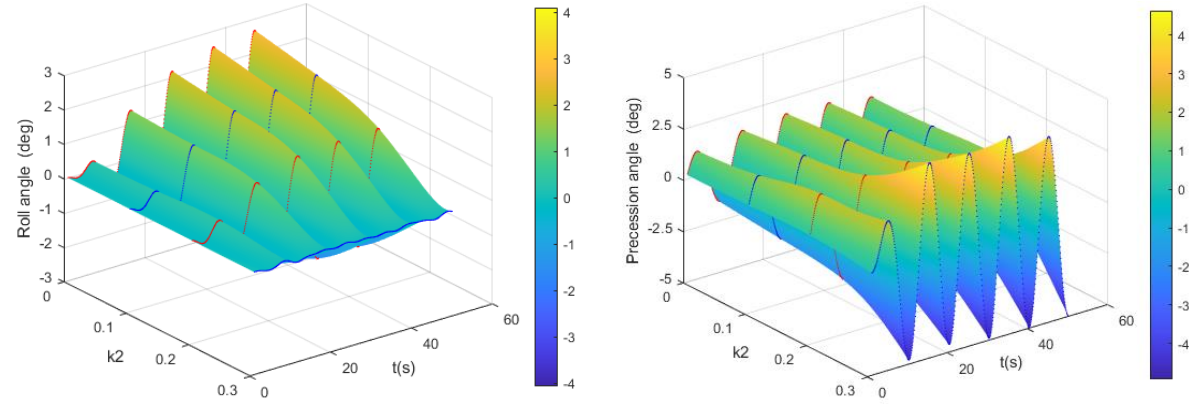

Fig. 10 Roll angle and precession angle amplitude change with k_2 for k_1=0.7 (left) roll angle; (right) precession angle.

On the other hand, the changes in precession angle with respect to weight k_2 under different k_1 are depicted in Fig. 9 and Fig. 10. The precession angle exhibits a periodic response pattern to the regular wave conditions, ranging from approximately -4 degrees to 4 degrees for $k_1 = 0.1$, and expanding to about -4.5 degrees to 4.5 degrees for $k_1 = 0.7$, with the peak average at about 3.413 degrees and 3.672 degrees respectively, as shown in Table 6. For a fixed k_1, the trend indicates that the precession angle increases with k_2. Initially, when k_2 is small, the change in precession angle is moderate, but as k_2 becomes larger, the variation becomes more pronounced. The precession angle increases sharply when k_2 reaches its limit due to no constrain on the control moment. Because of the regular wave action, both the roll angle and precession angle exhibit consistent behaviour.

Table 5 Maximum magnitude and peak's average of roll angle and precession angle result for regular wave ($k_1 = 0.1$)

Weights	**Value**	**Particulars**			
		Roll angle (deg)		Precession angle (deg)	
		maximum	peak's average	maximum	peak's average
k_2	0	4.106	2.181	1.040	0.664
	0.1	4.091	2.174	1.042	0.610

0.2	4.069	2.164	1.045	0.620
0.3	4.047	2.153	1.048	0.629
0.5	3.963	2.113	1.068	0.668
0.7	3.731	2.004	1.163	0.777
0.9	0.481	0.329	4.265	3.413

Table 6 Maximum magnitude and peak's average of roll angle and precession angle result for regular wave ($k_1 = 0.7$)

Weights	**Value**	**Particulars**			
		Roll angle (deg)		Precession angle (deg)	
		maximum	peak's average	maximum	peak's average
k_2	0	2.660	1.511	1.736	1.327
	0.1	2.281	1.338	1.994	1.541
	0.2	1.646	1.048	2.456	1.942
	0.3	0.081	0.033	4.644	3.672

The average peak values for different weights are presented in Fig. 11. In addition to peak values, trough data are also included to enhance data integrity. In the left panel of Fig. 11, the initial roll angle is noted to be approximately 10.25 degrees, which represents its maximum. As k_1 increases, the roll angle decreases sharply, indicating a strong dependence on k_1. Conversely, when k_1 is held constant, the roll angle changes more gradually with k_2, suggesting that the roll angle exerts dominant control compared to the reactive moment. The diagonal shadow signifies the minimal roll angle achieved under the current conditions. The right panel of Fig. 11 illustrates that the maximum precession angle is attained at the diagonal position. Furthermore, as k_1 increases, the average peak value of the precession angle also increases, reaching 5 degrees when $k_1 = 1$ and $k_2 = 0$. This quantitative result aligns with our hypothesis, indicating that the optimization process has identified an optimal solution for minimizing roll motion while maximizing precession angle adjustment. Thus, the parameters chosen for this study are deemed reasonable, and the control process and methods appear stable under regular wave conditions. Moreover, varying weights of k_1 and k_2 yield different control effects, offering flexibility in controlling motion according to specific application requirements. This flexibility can be particularly useful for fine-tuning motion control, potentially saving energy and costs while preventing structural damage.

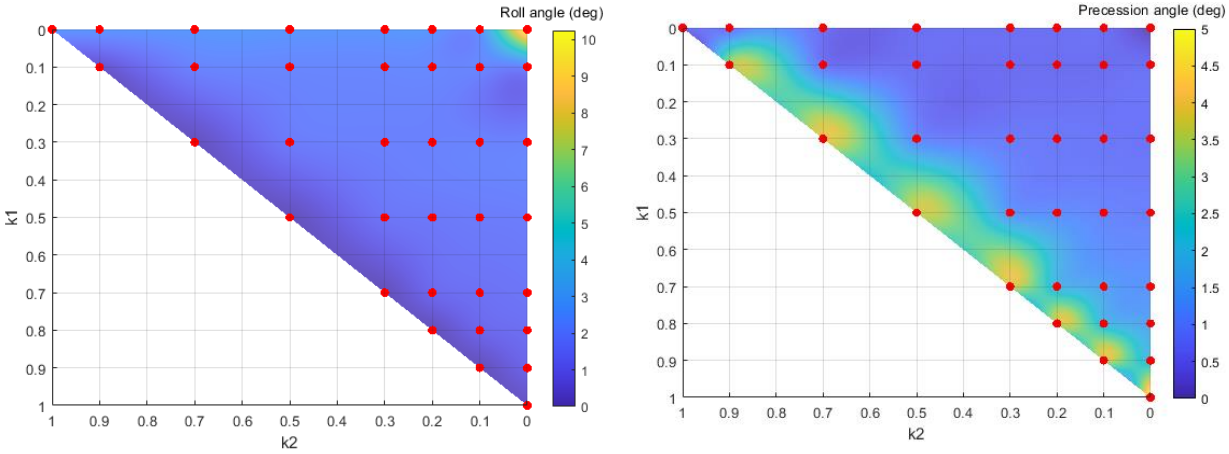

Fig. 11 The peak value's average for different weights (left) roll angle; (right) precession angle

4.3 Case study with irregular wave

Expanding on the analysis of regular wave, the control strategy is extend to irregular wave conditions. The wave moment is modelled as a stochastic process using the JONSWAP spectrum, detailed in Table 7. Fig. 12 depicts the roll motion response in the time domain. Specifically, the analysis focuses on the time interval between 100s and 150s, highlighted in the blue box.

Table 7 Wave parameters

Wave type	Wave parameters	Value
Irregular beam wave	spectrum	JONSWAP
	ω_p (rad/s)	0.885
	H_S (m)	6
	γ	1

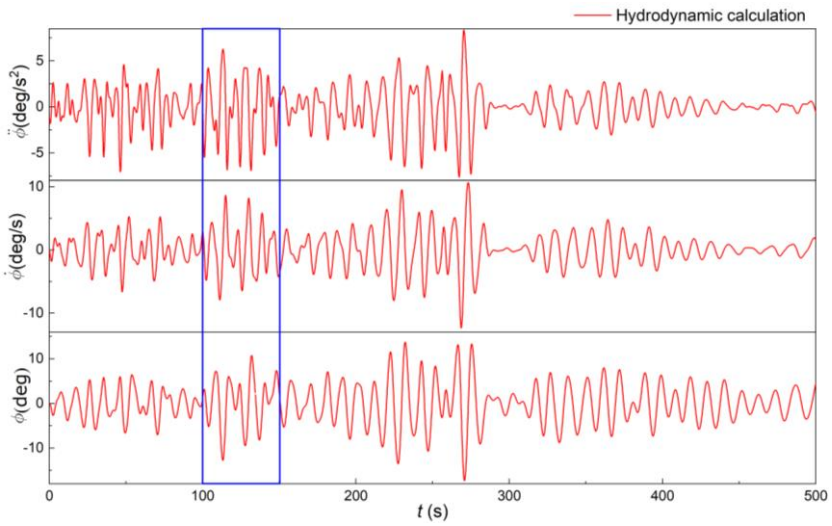

Fig. 12 Roll motion response (random wave, H_S=6m, ω_p=0.885 rad/s).

Due to the stochastic nature of irregular waves, the resulting conditions lead to unpredictable motion responses of the ship. Additionally, the precession of the gyrostabilizer can be affected under these conditions. Consequently, the roll angle variations with different k_1 exhibit irregularities. However, the overall tendency is analogous to that observed under regular wave conditions. Table 8 lists the peak average and maximum values of the roll angle and precession angle. During the 50-second control process, for $k_1 = 0.1$ as depicted in Fig. 13, the roll angle ranges from approximately -6.6 degrees to 6.6 degrees, gradually decreasing until $k_2 = 0.9$ where the peak average reduces significantly to 1.790 degrees. Simultaneously, the precession angle continues to increase, ranging from -20 degrees to about 25 degrees, with a maximum of 24.990 degrees and a peak average of 14.679 degrees. Conversely, under $k_1 = 0.7$, as shown in Fig. 14, the roll angle ranges from -2.5 degrees to 3.2 degrees, achieving a minimum of about 0.799 degrees and a peak average of 0.308 degrees at $k_2 = 0.3$. Correspondingly, the precession angle reaches its maximum at 36.365 degrees with a peak average of 19.501 degrees, as detailed in Table 9. The tendencies of roll angle and precession angle changes under random wave conditions mirror those observed under regular waves, whether assessed by maximum values or peak averages.

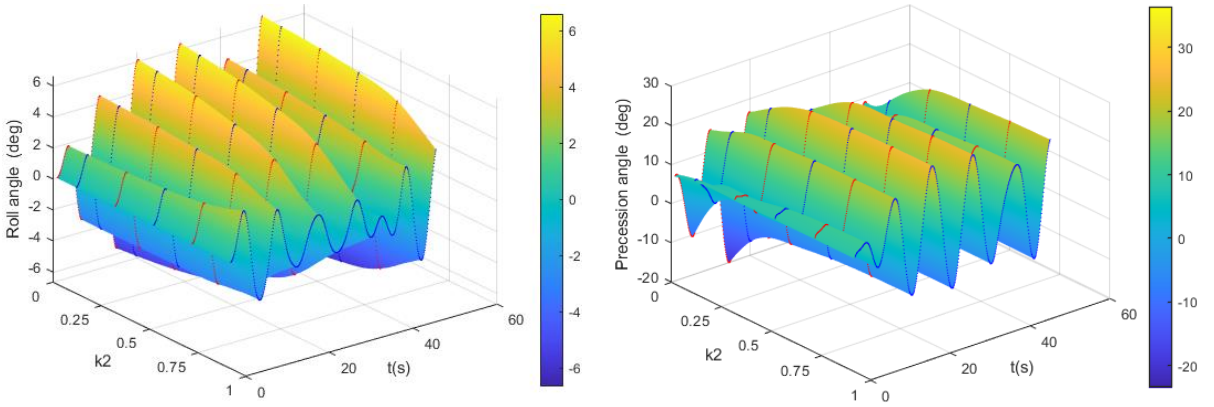

Fig. 13 Roll angle and precession angle amplitude change with k_2 (k_1 =0.1) (left) roll angle; (right) precession angle.

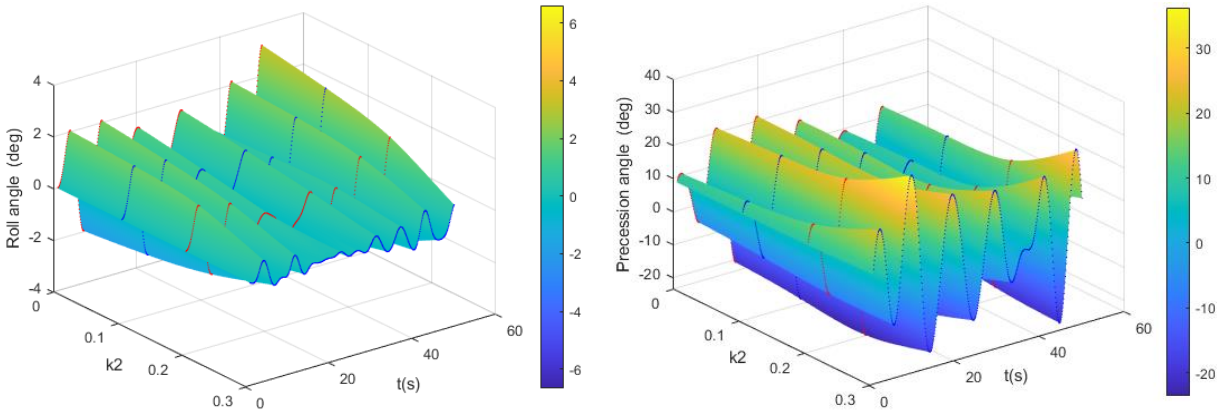

Fig. 14 Roll angle and precession angle amplitude change with k_2 for k_1 =0.7 (left) roll angle; (right) precession angle.

Table 8 Maximum magnitude and peak's average of roll angle and precession angle result for irregular wave ($k_1 = 0.1$)

Weights	**Value**	**Particulars**			
		Roll angle (deg)		Precession angle (deg)	
		maximum	average of peak	maximum	average of peak
k_2	0	6.604	4.176	16.554	13.114
	0.1	6.532	4.102	19.87	13.233
	0.2	6.432	4.003	23.997	13.471
	0.3	6.333	3.904	24.625	14.342
	0.5	6.002	3.595	24.767	14.4635
	0.7	5.375	3.314	24.909	14.585
	0.9	3.463	1.790	24.990	14.679

Table 9 Maximum magnitude and peak's average of roll angle and precession angle result for irregular wave ($k_1 = 0.7$)

Weights	**Value**	**Particulars**			
		Roll angle (deg)		Precession angle (deg)	
		maximum	average of peak	maximum	average of peak
k_2	0	3.199	1.654	21.419	15.155
	0.1	2.759	1.328	22.821	15.869
	0.2	2.090	1.015	25.610	17.169
	0.3	0.799	0.308	36.365	19.501

Fig. 15 illustrates the average peak values for different weights, where the left panel shows the roll angle and the right panel represents the precession angle. In the left panel shadow, it is evident that the roll angle decreases along the diagonal line, reaching its maximum when k_1 and k_2 are zero. Generally, as k_1 increases, the roll angle decreases noticeably. Conversely, the trend is less pronounced when k_2 increases, indicating that the weight of k_1 has a more sensitive impact on the control effect. This phenomenon is also reflected in the precession angle shown in Fig. 15, where it peaks at approximately 45 degrees when $k_1=1$. With the condition where $k_2=1$, the precession angle decreases to around 6.5 degrees, which is smaller than that observed with $k_1=1$. Throughout this process, adjusting the weights of k_1 and k_2 allows for flexible intermediate control effect, helping to avoid energy waste and structure damage in roll motion control scenarios. The results from both regular and irregular wave motion control indicate that different motion control effects can be achieved by adjusting the weights of roll angle, control moment, and reactive moment. Furthermore, the observed trends under irregular waves closely mirror those under regular waves, demonstrating that the proposed multi-objective model predictive control and gyrostabilizer methods, provides a versatile control strategy under varying wave conditions. This approach can effectively control ship roll motion according to user requirements, regardless the waves are regular or irregular.

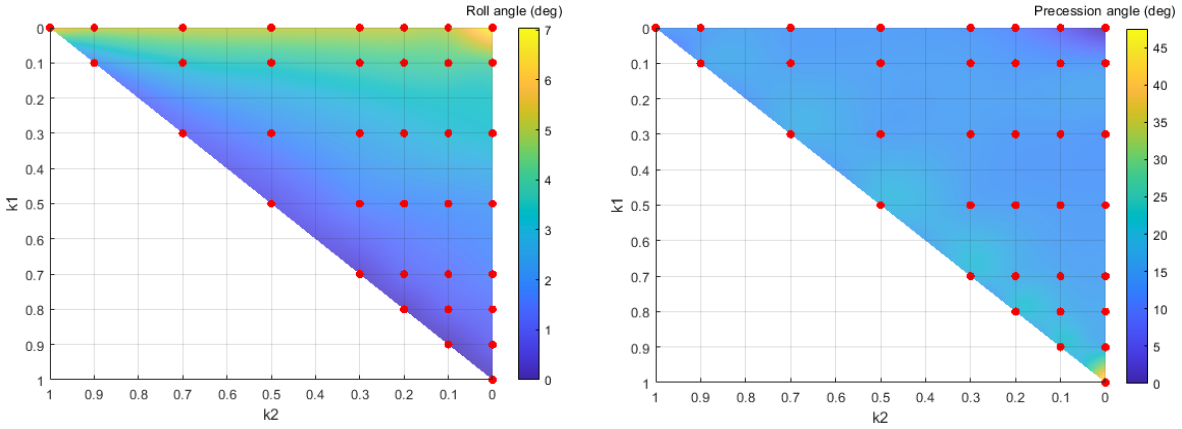

Fig. 15 The peak value's average for different weights (left) roll angle; (right) precession angle.

5 Conclusions

This study introduces a multi-objective cost function for the evaluation of the roll motion control performance based on the combination of MPC and gyrostabilizer, and considering the retardation effects of waves. Unlike previous investigations, this multi-objective model predictive control approach integrates considerations of roll motion, potential structural damage, and energy consumption to conduct the operation by assigning different weights to each factor. Consequently, the proposed method offers flexible control capabilities tailored to user requirements, based on solutions derived from nonlinear dynamic models. The study accomplishes roll motion adjustment for a frigate model under different wave conditions. It compares the maximum amplitudes and average peak values of roll angle and precession angle across different weight configurations. The analysis explores the changing trends observed under various weights in both regular and irregular wave scenarios. It examines different control effects and provides explanations for observed outcomes.

Results indicate that the multi-objective model predictive control approach, with its assigned weights, effectively reduces roll motions to small degrees. This analysis offers valuable insights into managing roll motion in challenging wave states and proposes a practical approach in the field of ship motion control, thereby contributing to advancements in maritime engineering practices.

The current research primarily concentrates on analyzing the model framework in theory. However, it exhibits certain limitations, such as the linearization of nonlinear restoring terms in state-space model solutions and a lack of experimental validation. Future work will explore the discrepancy caused by linearization further to ensure the accuracy in a higher level, and involve conducting related experimental research on combined systems implemented in real ships. Moreover, predicting future wave moments is crucial for real-time control in ships, and efforts are underway to achieve this using artificial neural networks. Furthermore, the analysis thus far has primarily focused on 1-degree-of-freedom (1-DOF) roll motion control. Future investigations will explore the coupling of roll motion with other directional motions such as pitch and heave under irregular beam waves.

Declaration of competing interest

The authors declare that they have no known competing financial interests or personal relationships that could have appeared to influence the work reported in this paper.

CRediT authorship contribution statement

Lifen Hu: Methodology, Writing - review & editing, Writing - original draft, Formal analysis. **Ming Zhang**: Writing - review & editing. **Gang Li**: Software, Investigation. **Zhiming Yuan**: Investigation, Writing - review & editing. **Junying Bi**: Data curation. **Yanli Guo:** Writing - review & editing.

Acknowledgments

This study was supported financially by the National Natural Science Foundation of China (Grant No. 52371325), the Natural Science Foundation of Shandong Province (Grant No. ZR2020ME263), the Fundamental Research Funds for the Central Universities (Grant No. 3072024XX0107). The authors extend their sincere gratitude to the abovementioned organizations.

References

Afram, A., Janabi-Sharifi, F., 2014. Theory and application of HVAC control systems – A review of model predictive control (MPC), Building and Environment, 72, 343-355.

Aswani, A., Master, N., Taneja, J., Culler, D., Tomlin C., 2012. Reducing transient and steady state electricity consumption in HVAC using learning-based model predictive control. Proc of the IEEE, 100, 240-253.

Begovic, E., Mortola, G., Incecik, A., Day, A. H., 2013. Experimental assessment of intact and damaged ship motions in head, beam and quartering seas. Ocean Engineering, 72, 209-226.

Bu, S., Gu, M., 2020. Unified viscous and potential prediction method for the coupled motion of damaged ship and floodwater in calm water. Ocean Engineering, 210, 107441.

Chu, T., Chen, C., 2017. Design and Implementation of Model Predictive Control for a Gyroscopic Inverted Pendulum, Applied Sciences, 7(12), 1272.

Cummins, W., 1962. The impulse response function and ship motions. Schiffstechnik, 9, 101-109.

Fossen, T., Handbook of Marine Craft Hydrodynamics and Motion Control. Norway: John Wiley & Sons Ltd, 2011.

Findeisen, R., Allgöwer, F., 2002. An introduction to nonlinear model predictive control, 21st Benelux Meeting on Systems and Control, The Netherlands: 119–141.

Gao, Z., Wang, Y., Su, Y., 2020. On damaged ship motion and capsizing in beam waves due to sudden water ingress using the RANS method. Applied Ocean Research, 95, 102047.

Hinostroza, M., Luo, W., Soares, C.G., 2015. Robust fin control for ship roll stabilization based on l2-gain design. Ocean Engineering, 94, 126-131.

Hu, L., Li, W., Lu, J., 2018. Research on capsizing probability of stability under dead ship condition in beam wind and wave. Chinese Journal of Hydrodynamics, 33(6), 794-800.

Hu, L., Wu, H., Yuan, Z., Li, W., Wang, X., 2021. Roll motion response analysis of damaged ships in beam waves. Ocean Engineering, 227, 108558.

Hu, L., Zhang, M., Yuan, Z., Zheng, H., Lv W., 2023a. Predictive Control of a Heaving Compensation System Based on Machine Learning Prediction Algorithm. Journal of Marine Science and Engineering, 11(4), 821.

Hu, L., Zhang, M., Yu, X., Yuan, Z., Li, W., 2023b. Real-time control of ship's roll motion with gyrostabilizers. Ocean Engineering, 285, 115348.

Irkal, M., Nallayarasu, S., Bhattacharyya, S., 2019. Numerical prediction of roll damping of ships with and without bilge keel. Ocean Engineering, 179, 226-245.

Jimoh, I. A., Küçükdemiral, I. B., Bevan, G., 2021. Fin control for ship roll motion stabilisation based on observer enhanced MPC with disturbance rate compensation, Ocean Engineering, 224, 108706.

Kang, E., Qiao, H., Gao, J., Yang, W., 2021. Neural network-based model predictive tracking control of an uncertain robotic manipulator with input constraints. ISA Transactions, 109, 89-101.

Kang, H., Yang, Y., Choi, J., Lee, Jong., Lee, Dong., 2013. Time basis ship safety assessment model for a novel ship design. Ocean Engineering, 59, 179-189.

Kucukdemiral, I. B., Cakici, F., Yazici H., A model predictive vertical motion control of a passenger ship, Ocean Engineering, 2019, 186, 106100.

Ławryńczuk, M., Nebeluk, R., 2023. Beyond the quadratic norm: Computationally efficient constrained nonlinear MPC using a custom function, ISA Transactions, 134, 336-356.

Lee, S., Rhee, K., Choi, J., 2011. Design of the roll stabilization controller, using fin stabilizers and pod propellers. Applied Ocean Research, 33(4), 229-239.

Li, R., Li, T., Bai, W., Du, X., 2016a. An adaptive neural network approach for ship roll stabilization via fin control. Neurocomputing, 173, 953-957.

Li, Y., Zhu, R., Miao, G., Fan, J., 2016b. Numerical method of ship motions coupled with tank sloshing based on fully time domain potential flow theory. Journal of Ship Mechanics, 20(11), 1369-1380.

Li, W., Sun, Y., Chen, H., Wang, G., 2017. Model predictive controller design for ship dynamic positioning system based on state-space equations. Journal of Marine Science and Technology, 22, 426-431.

Li, L., The development of a realtime wave energy device control algorithm based on artificial neural network. Scotland: University of Strathclyde, 2018.

Li, L., Liu, Y., Yuan, Z., Gao, Y., 2019. Dynamic and structural performances of offshore floating wind turbines in turbulent wind flow. Ocean Engineering, 179, 92-103.

Liu, C., Wang, D., Zhang, Y., Meng, X., 2020. Model predictive control for path following and roll stabilization of marine vessels based on neurodynamic optimization. Ocean Engineering, 217, 107524.

Liu, Y., Xia Z., Tang Y., Zhang J., Fan S., 2022. Research on the ship roll stabilization with gyrostabilizer. Preceedings of the 3rd National Conference on Stability of Ships, 211-215, Shanghai, China.

Ma, H., Zhang, Y., Wang, S., Xu, J., Su, H., 2022. Rolling-optimized model predictive vibration controller for offshore platforms subjected to random waves and winds under uncertain sensing delay, Ocean Engineering, 252, 111054.

Palraj, M., Rajamanickam, P., 2020. Motion control of a barge for offshore wind turbine (OWT) using gyrostabilizer. Ocean Engineering, 209, 107500.

Palraj, M., Rajamanickam, P., 2021. Motion control studies of a barge mounted offshore dynamic wind turbine using gyrostabilizer. Ocean Engineering, 237, 109578.

Pascoal, R., Rodrigues, B., Soares, C.G., 2005. Roll-yaw regulation using stabilizing fins and rudder in a disturbance observer based compensator scheme. Maritime Transportation and Exploitation of Ocean and Coastal Resources, Two Volume Set. CRC Press, pp. 740-747.

Perez, T., Steinmann, P. D., 2009a. Analysis of Ship Roll Gyrostabiliser Control. Proceedings of the 8th IFAC International Conference on Manoeuvring and Control of Marine Craft, 310-315, Guaruj á, Brazil.

Perez, T., Fossen, T., 2009b. A Matlab Toolbox for Parametric Identification of Radiatioin-Force Models of Ships and Offshore Structures. Modeling, Identification and Control, 30(1), 1-15.

Sandeepkumar, R., Rajendran, S., Mohan, R., Pascol, A., 2022. A unified ship manoeuvring model with a nonlinear model predictive controller for path following in regular waves, Ocean Engineering, 243, 110165.

Shu, Y., Xiong, C., Zhu, Y., Liu, K., Liu, R., Xu, F., Gan, L., Zhang, L., 2024. Reference path for ships in ports and waterways based on optimal control, Ocean & Coastal Management, 253, 107168.

Song, K., Kim, S., Kwak, M., Zhu, W., 2023. Development of a control algorithm for active control of rolling motion of a ship using a gyrostabilizer, Ocean Engineering, 280, 114669.

Steinmann, P., VEEM, G., 2014. How Gyros Create Stabilizing Torque How Gyro s Creat Stabilizing Torque. VEEMGYRO. WWW Document.

Suner, M., Bas, M., 2022. A new approach to narrow waterways traffic routing with potential flow theory and CFD. Ocean Engineering, 261, 111862.

Taghipour, R., Perez, T., Moan, T., 2008. Hybrid frequency-time domain models for dynamic response analysis of marine structures. Ocean Engineering, 35(7), 685-705.

Takeuchi, H., Umemura, K., Maeda, S., 2011. Development of the anti rolling gyro 375T (rolling stabilizer for yachts) using space control technology. Mitsubishi Heavy Industries Technical Review, 48(4), 70-75.

Tiwari, K., Krishnankutty, P., 2021. Dynamic positioning of an oceanographic research vessel using fuzzy logic controller in different sea states. Marine Systems & Ocean Technology, 16, 221-236.

Townsend, N., Murphy, A., Shenoi, R., 2007. A new active gyrostabilizer system for ride control of marine vehicles. Ocean Engineering, 34, 1607-1617.

Townsend, N., Shenoi, R., 2014. Control Strategies for Marine Gyrostabilizers, IEEE Journal of Oceanic Engineering, 39(2), 243-255.

Tomera, M., 2017. Fuzzy self-tuning PID controller for a ship autopilot. Proceedings of the 12th International Conference on Marine Navigation and Safety of Sea Transportation, 93-103, Gdynia, Poland.

Zhang, X., Yang, J., Zhao, W., Xiao, L., 2016. Effects of wave excitation force prediction deviations on the discrete control performance of an oscillating wave energy converter. Ships Offshore Structure, 11(4), 351-368.

Zhang, M., Hao, H., Wu, D., Chen, M., Yuan, Z., 2022. Time-optimal obstacle avoidance of autonomous ship based on nonlinear model predictive control, Ocean Engineering, 266, 112591.

Zhang, M., Yu S., Zhao, G., Dai, S., He, F., Yuan, Z., 2024. Model predictive control of wave energy converters, Ocean Engineering, 301, 117430.